Experimental and Numerical Analysis of Diluted Combustion in a Direct Injection CNG Engine Featuring Post- Euro-VI Fuel Consumption Targets

2018-01-1142

Experimental and numerical analysis of diluted combustion in a direct injection CNG engine featuring post- Euro-VI fuel consumption targets

Author, co-author (Do NOT enter this information. It will be pulled from participant tab in MyTechZone)

Affiliation (Do NOT enter this information. It will be pulled from participant tab in MyTechZone)

Abstract

The present paper is concerned with part of the work performed by Renault, IFPEN and Politecnico di Torino within a research project founded by the European Commission. The project has been focused on the development of a dedicated CNG engine featuring a 25% decrease in fuel consumption with respect to an equivalent Diesel engine with the same performance targets. To that end, different technologies were implemented and optimized in the engine, namely, direct injection, variable valve timing, LP EGR with advanced turbocharging, and diluted combustion. With specific reference to diluted combustion, it is rather well established for gasoline engines whereas it still poses several critical issues for CNG ones, mainly due to the lower exhaust temperatures. Moreover, dilution is accompanied by a decrease in the laminar burning speed of the unburned mixture and this generally leads to a detriment in combustion efficiency and stability. The optimization of in-cylinder turbulence plays a fundamental role in compensating this trend.

The present paper is specifically focused on the characterization of the diluted combustion in the direct injection engine. The results of an experimental activity have been presented, aimed at characterizing the in-cylinder combustion process and the exhaust temperatures at 2000 rpm and variable load, both without dilution and with 20% of external EGR. At the same time, a 3-D numerical model for the in-cylinder turbulence and combustion simulation has been developed in Converge. The model embeds a user-specified laminar-flame speed submodel, which was derived from a 1-D combustion simulation model with detailed chemistry. The model has been calibrated against experimental data and then used to characterize the heat release dependence on the dilution. The experimental activity has evidenced the potential of EGR to increase the engine efficiency, by allowing to increase the boost level at full load and by reducing pumping losses at partial load. As far as the maximum allowed EGR rate is concerned, the CFD activity showed that the limit can be detected on the basis of a threshold value of the MFB0-50 interval. At 2000 rpm and medium load the maximum EGR rate ranged around 35% and showed an increasing trend versus load. It also demonstrated a decreasing trend against the engine speed.

Introduction and present work

Natural gas (NG) is considered one of the most promising alternative fuels, which can effectively cope with the reduction of the carbon footprint and emissions of vehicles, with respect to conventional IC engines [1,2]. As a matter of fact, methane is the primary constituent of NG. It has the highest molecular hydrogen-to-carbon ratio of all hydrocarbons, which allows a potential of 20% CO2 reduction as compared to the long-chained molecules found in Diesel oil and gasoline. Another attractive chemical property of methane is its research octane number of 130 which is considerably higher than that of gasoline. This indicates high knock resistance as a promising enabling factor for extracting more power from a given engine displacement and therefore increasing engine specific power. NG engines operating with high compression ratio and boost pressure level as well as lean-burn approach or heavy exhaust gas recirculation could be equivalent to their gasoline counterparts in terms of torque and power, allowing also a substantial reduction in pollutant emissions and improvement in engine thermal efficiency [1,3,4].

The objective of the project Gason ("Gas-Only internal combustion engines", H2020 innovation action of the European Commission) is to design an engine for passenger cars or small duty vehicles applications and to demonstrate the potential of CNG fuels in a dedicated design [5]. The work presented in this paper was carried out by Renault, IFPEN and Politecnico di Torino within the Gason WP4, "Charge dilution (lean burn, internal and / or external EGR) and exhaust-gas temperature management". Within this context the activity was aimed at studying the impact of the charge dilution with EGR on the combustion process.

The attractiveness of diluted combustion is connected to its potential to improve the global efficiency of the engine [6]. Although this technology is relatively new for CNG engines, a few interesting works can be found in the literature [7-11]. Zoldak and Naber [7] performed an extensive experimental analysis of diluted combustion in a HD CNG engine. They found a good combustion stability up to EGR=20%, and a maximum indicated gross thermal efficiency of 45% was achieved. McTaggart-Cowan et al. [8] analyzed the influence of fuel composition on EGR tolerance and found that the influence of the percentage range of the lower hydrocarbon molecules is relatively small. Reduction in ignition delay at constant combustion phasing leads to lower peak heat release rates. However, these changes are not large enough to significantly impair engine operations. Morteza Fathi et al. [9] investigated the HCCI combustion of a n-eptane/CNG blend and used EGR rate to control autoignition time, flame-propagation speed and peak-pressure rise rate. These findings are useful also in view of EGR adoption in a more conventional spark-ignited engine. Despite the already mentioned high resistance of CNG to abnormal combustion, the current limitation to the achievable boost level is the maximum

temperature acceptable by the turbine, amongst other factors. Consequently, combustion dilution is a promising solution to keep the exhaust temperature below the safety limit of the turbine, and can improve the global efficiency of the engine. moreover, a dethrottling effect can be obtained at partial load, which also contributes to enhance the engine efficiency [7]. However, charge dilution can also lead to severe combustion problems, such as cycle-to-cycle variation and, for high dilution levels, misfire events.

Starting from the previous experience of the partners in the Mogador and InGAS projects [12,13], the engine performance and combustion features with diluted combustion were investigated in this work. First, the results of an experimental activity are presented in the paper, aimed at characterizing the in-cylinder combustion process and the exhaust temperatures in the Gason engine, for different engine speeds, loads, as well as injection timings. At the same time, an accurate 3-D numerical model for the in-cylinder turbulence and combustion simulation has been developed in the Converge software.

Test engine

The CNG direct injection engine under study has been developed by Renault. The engine performance were predicted based on previous results of the Mogador project [12], and the target of 125 kW and 380 Nm seemed to be reasonable for a 1,6 liter engine. The main features of the Gason engine are listed in Table 1.

Table 1. Main engine characteristics

Set-up	
Number of cylinders	4
Displacement	1.6 l
Number of valves / cylinders	4
Bore / stroke	80 mm / 80 mm
Compression ratio	13.5:1
Peak pressure	180 bar
Direct injection / Injection pressure	20 bar

Thanks to the fuel characteristic and knock resistance benefit of CNG it was possible to increase the compression ratio to 13.5:1. This allows a great effect to be obtained for the thermal efficiency of the engine. However, this high level of compression ratio increases the maximum peak pressure of combustion up to 180 bars and oriented to the design of a diesel-based engine. The revision of the combustion chamber design also involved the geometry of the intake ports associated to a variable valve timing (VVT) on both intake and exhaust camshafts, in order to maximize the tumble-generated in-cylinder turbulence and thus increase the engine dilution tolerance. The geometry of the combustion chamber is shown in Figure 1. The tests were carried out on a single cylinder version of the Gason engine, with a 405 cm^3 displacement and a compression ratio of 13.4:1 (Table 2). The intake and exhaust valve lift laws and timings were taken nearly the same as in the Mogador project for comparison. The piston had a central shallow bowl facing the injector and the spark plug. This piston design had already proved its potential and remained similar to the one of [12].

Table 2. Single cylinder engine characteristics

Engine displacement	405 cm^3
Bore / Stroke	80 mm / 80.5 mm
Compression ratio	13.4:1
Piston	Central shallow bowl
Ignition system	Mercedes Coil (90 mJ) NGK spark plug (ILZKR8A)
Intake valve	Opening duration = 169 CAD / maximum lift = 8.5 mm IVO = -6 ATDC / IVC = -5 ABDC
Exhaust valve	Opening duration = 200 CAD / maximum lift = 8.5 mm EVO = +38 BBDC / EVC = -18 BTDC
Fuel system	Continental CNG-DI prototype
Engine limits	Average max. cylinder pressure = 160 bar Average max. cylinder pressure + 2σ = 180 bar Max air pressure = 3 bar Maximum exhaust temperature = 850°C

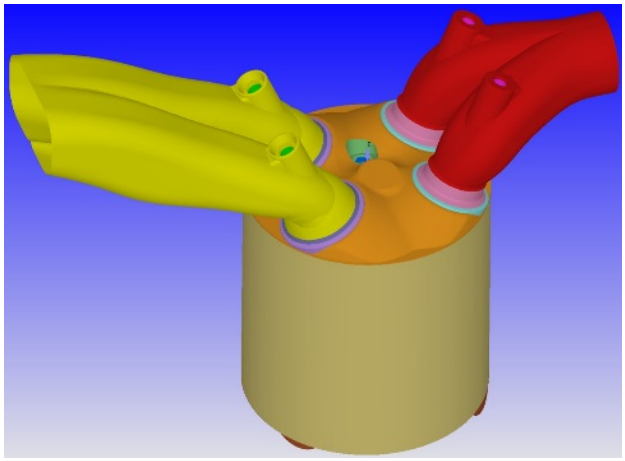

Figure 1. Combustion chamber of the Gason engine.

Experimental setup

In order to carry out the experimental activity, the single-cylinder engine (SCE) was equipped with a prototype direct injection system, which was developed by Continental along with its control box. The rate of fuel consumption was measured by a MicroMotion CMF010 Coriolis type mass flow meter.

The layout of the engine installation is shown in Figure 2. Turbocharged conditions were simulated with a set of chocked flows that allows regulation and measurement of the air flow. An air heater was implemented on the circuit to simulate the air temperature induced by the compressor and regulated by the air cooler. The exhaust backpressure was set using an exhaust throttle which was regulated in position, to match with the exhaust back pressure generated by all the restrictions along the actual MCE exhaust line (turbine, after treatment device, muffler,…). LP-EGR conditions

were simulated with a set of a valve, double compressors and exchangers that allowed the regulation of exhaust gas flow and temperature and their measurement.

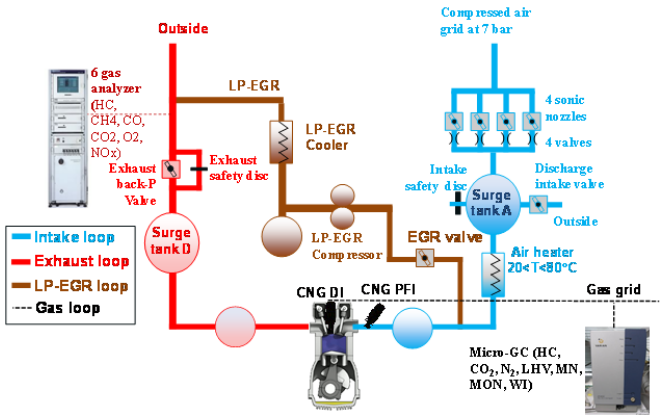

Figure 2. Single-cylinder engine installation on the test bench.

In-cylinder pressure was monitored by a flush mounted cooled AVL QC34D pressure transducer. The pressure signal was acquired for every 0.1 CAD and the acquisition process covered 100 complete cycles. The average value of these cycles was used as pressure data for the calculation of combustion parameters. Engine-out exhaust gases (HC, CH4, CO, CO2, O2, NOx) were analyzed by an AVL AMA4000 analyzer.

Table 3. Average CNG properties.

Properties	CNG (average)
Lower heating Value (MJ/kg)	47.0 ± 2.1
Methane (% mass)	91.95 ± 0.55
Ethane (% mass)	4.54 ± 0.23
Propane (% mass)	0.59 ± 0.13
Nitrogen (% mass)	1.09 ± 0.13
H/C (mol/mol)	3.82 ± 0.01
Stoichiometric AFR (kg/kg)	16.1 ± 0.1
MON	126 ± 1

Commercial grid CNG was used in this study. The fuel properties were monitored during the tests and proved to be very stable (see Table 3). Tests at full load were performed at the targeted IMEP and engine differential pressure assessed to achieve the desired performance and to respect the engine mechanical and thermal limits. Tests at part load were operated at the exhaust throttle position identical to the full load one for each selected engine speed.

CFD model

To help to investigate combustion efficiency and determine the impact of the charge dilution, a complete modeling of the CNG engine fluid-dynamics and combustion was implemented in the CONVERGE code. The simulation objective was to develop a numerical model for 3D simulation and to validate simulation results with the experimental data of in-cylinder pressure at different engine operating points (engine speed and load). The validated model was then used to predict the combustion behavior with EGR.

The starting point of the CFD model development was the engine geometry data (Fig. 1). The unique property of the CONVERGE software is that it automatically generates perfectly orthogonal, block-structured grid at runtime based on the user defined grid parameters. The length of the intake and exhaust pipe portions to be included in the model was defined keeping in mind the position of pressure transducers in the experimental setting. The boundary conditions were applied based on proper surface or region definitions. In the cases for which experimental tests were available for model validation, the experimental value of pressure (time-dependent) and temperature (constant, time-averaged, value) was imposed as boundary condition at the intake and exhaust ports end. A low-pass filter with cut-off frequency of 5 kHz was used to remove the noise. When experimental data were not available, the necessary boundary conditions were applied based on a 1-D engine simulation in GT-Power. Other boundary conditions are defined based on the nature of surfaces, for example, wall translating boundary to piston and valves, wall fixed boundary to cylinder head and liner.

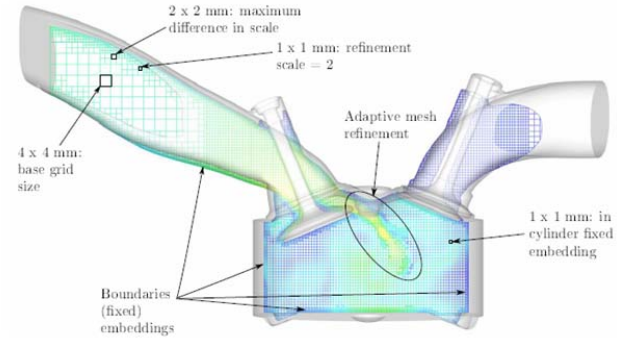

Figure 3. Grid settings and adaptive mesh refinement in the engine CFD model.

Table 4. Fixed embedding setting for the engine CFD mesh refinement.

Place	Type	Temporal type	Grid scaling factor	Grid size [mm]
Cylinder	cylinder	Permanent	2	1
Intake Port	boundary	cyclic (720 cad)	3	0.5
Intake Valve	boundary	cyclic (720 cad)	3	0.5
Piston	boundary	Permanent	3	0.5
Liner	boundary	Permanent	3	0.5
Cylinder Head	boundary	Permanent	3	0.5
Exhaust Valve	boundary	cyclic (720 cad)	3	0.5
Spark 1	sphere	cyclic (720 cad)	3	0.5
Spark 2	sphere	cyclic (720 cad)	5	0.125

Table 5. Numerical setup summary.

Flow	Compressible Flow
Gas Simulation	Redlich Kwong model
Numerical method	Implicit method
Turbulence model	RNG k-ε
Combustion model	ECFM
Heat transfer model	WF - Angelberger

Figure 3 shows an example of the grid, which was generated by the code by applying the user settings. The base mesh grid, as shown in the figure, is of 4 x 4 mm. To refine the grid size, different scaling methods were used as described in Table 4. The attractive Adaptive Mesh Refinement (AMR) facility was applied on different regions to automatically refine the grid based on the gradients of the main flow variables, such as, velocity and temperature. The main numerical setup physical model selection is reported in Table 5.

In this paper, combustion modeling was based on a premixed flame hypothesis, and a perfectly uniform mixture was considered at the engine intake. This assumption was justified by the very early injection timings that were actuated. In such conditions, both the preliminary experimental data provided by IFPEN and the available literature ([14]) assess for a high degree of fuel-air homogeneity. The different combustion regimes of premixed flames are well described in the Borghi and Peters diagram [15]. Preliminary study based on aerodynamic simulation helped to make a reasonable estimation of the turbulence and of the laminar flame speed, thus confirming the validity of the corrugated flame regime in this case. From these results, the ECFM model (Extended Coherent Flame Model, [16]) was selected. ECFM is based on the idea that the turbulent flame is a collection of single elements, each behaving as laminar flame ('flamelet' assumption). The flame surface density is defined by the following transport equation:

$$\frac{\partial \Sigma}{\partial (t)} + \frac{\partial u_{f_i} \Sigma}{\partial x_i} = \frac{\partial}{\partial x_i}\left(\frac{\mu}{Sc_t}\frac{\partial \Sigma/\rho}{\partial x_i}\right) + (P_1 + P_2 + P_3) - D + P_k \qquad (1)$$

where $P_1 = \alpha K_t$ represents the flame surface density production by turbulent stretch, and α is a calibration parameter. It is worth pointing out that, in general, the model results might be affected by the absence of the fuel injection simulation [17-19]. However, due to the very early injection timings, the influence of the fuel jet on the in-cylinder tumble and turbulence can be neglected ([14]). Consequently, the turbulence field given by the model is also representative of the direct gas injection case.

The Imposed Stretch Spark Ignition Model (ISSIM, [20]) is also used as ignition submodel. This model simultaneously represents both the electrical circuit energy deposition and flame surface and mass deposition. The calibration parameter for ISSIM is C_{surf} that corresponds to an initial wrinkling value for the flame. It allows the non-perfect sphericity of the flame kernel to be accounted for. The ECFM model structure requires that the laminar flame speed (LFS) is given as an input. To that end, in order to improve the model accuracy, a detailed model based on a reaction mechanism (GRI Mech 3.0, [21]) was developed for the specific fuel composition used

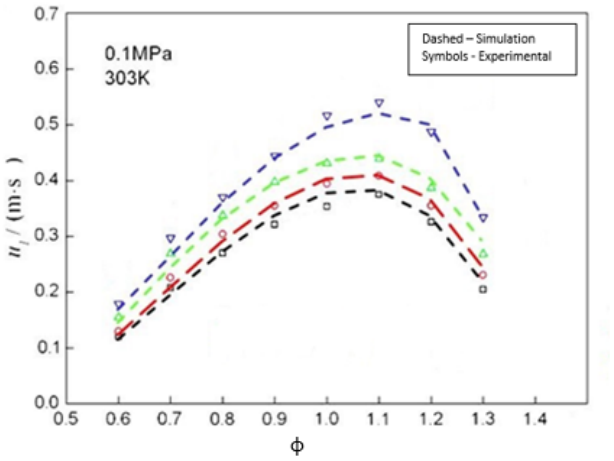

Figure 4. Validation of the LFS submodel dashed black: 100% CH_4, dashed red: blend with 10% H_2, dashed green: blend with 20% H_2, dashed blue: blend with 30% H_2.

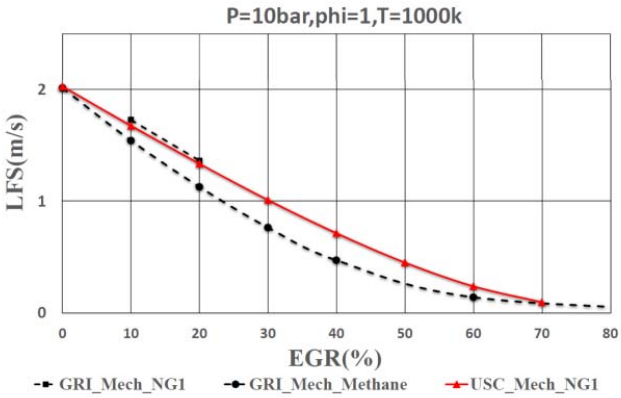

Figure 5. LFS against EGR at given thermodynamic conditions and λ = 1.0.

in the experimental tests. The model outcomes were organized in the form of a look-up table as a function of dependent variables (pressure, temperature, EGR rate and equivalence ratio) and then implemented in the model via user-defined function. The benefits of using this method are twofold. First, accurate laminar flame speed estimation over a wide range of dependent variables which can hardly be achieved by using empirical relations [22, 23]. Second, reduction in computation time and cost with respect of solving kinetic reactions and the relative scalar variables embedded in the model. Figure 4 shows the validation of LFS model with respect to experimental data taken from [24]. Two mechanisms had been initially tested, GRI Mech 3.0 and USC Mech II [25]. LFS calculations were performed for pure methane and NG composition, and both mechanisms behaved similarly in most of the cases for a given fuel composition. As GRI Mech 3.0 has been widely used and is validated by various researchers under engine-like conditions [26-28], it was finally selected in this work. The GRI-Mech accuracy was found to be within 15%, although a correction in the original mechanism was necessary for pressure higher than 40 bar [27]. More information about the laminar flame speed submodel are provided in a companion paper, currently under preparation. Finally, Fig. 5 shows the LFS against EGR rate, obtained for both pure methane and 'NG1', which is the gas composition considered in the Gason WP4 engine

development. As can be seen, LFS of pure methane is lower than for natural gas, and the difference is higher EGR % increases. This is consistent with the lower reactivity of pure methane with respect to natural gas, in which non-negligible quantities of ethane and propane are present.

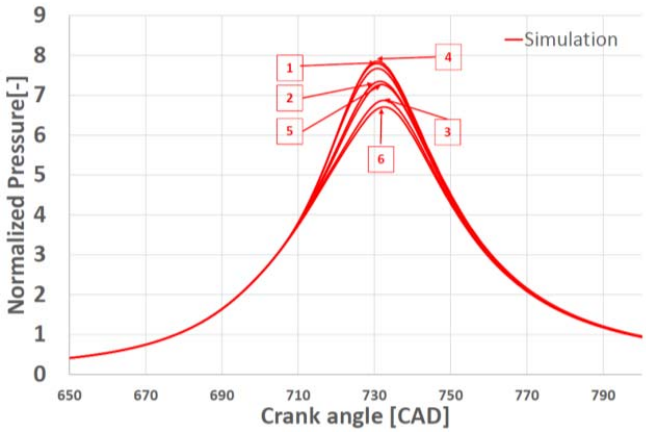

Figure 6. Cycle-to-cycle variation in the engine simulation.

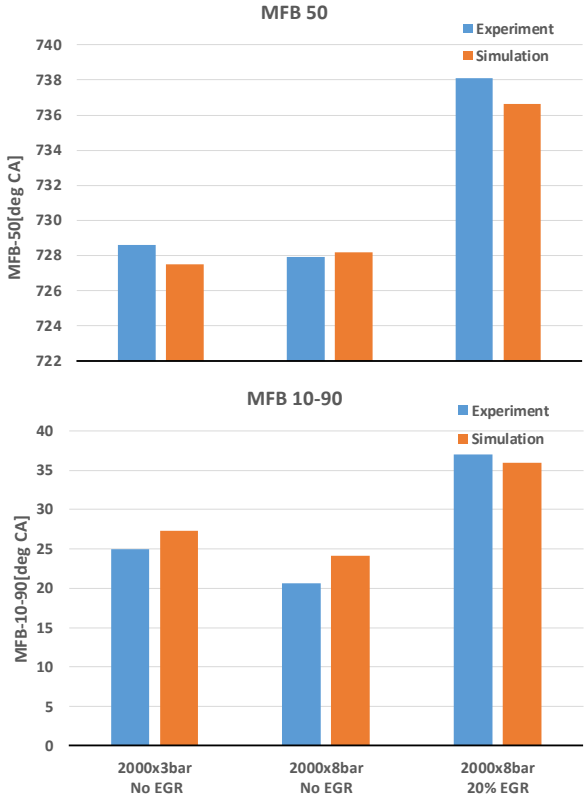

Figure 7. CFD model validation: combustion-related indicators for different working conditions.

Following the indications in [12, 29], multi-cycle simulations were arranged in this work, in order to obtain more reliable results. However, in many working conditions, it was not possible to reach a stable cycle-to-cycle evolution. This behavior has been already mentioned in the literature, and is attributed to the quite fine grid adopted, and to the AMR strategy, which decrease the grid numerical viscosity to a great extent [30, 31]. Figure 6 represents an example of this behavior. Following the suggestions found in [30, 31], in order to reach conclusive and significant results, 7 cycles were run for each condition, and an ensemble operation among the cycles from no.2 to no.7 was carried out to derive the presented results. Cycle no.1 was considered as affected by the initial conditions and thus was discarded. Once the model had been calibrated with reference to the working conditions without EGR, the cases with EGR were simulated by using the same model coefficients.

Model validation

The model was validated against experimental data, with reference to the cases without EGR, in the 2000x3 and 2000x8 working conditions (the first number indicates the engine speed in rpm, the second one is the engine imep in bar). The coefficients α and C_{Surf}, mentioned in the previous sections, were calibrated for this purpose. The coefficients were calibrated for each point in the absence of EGR, and then kept constant as EGR was changed in the simulations. The results of the model validation are shown in Figs. 7-9. Along with the in-cylinder pressure, the heat release was considered for the validation. The latter was derived from the experimental and the numerical pressure curve by applying the single-zone heat release model proposed by Brunt et al. [32]. Due to confidentiality issues, the pressure curves have been normalized to a specific reference value, which has been kept constant for all the pressure curves. The model shows a generally good agreement with the experimental results. The main combustion angles are reproduced with an error lower than 2 deg, with the only exception of the MFB10-90 interval for the 2000x8 case without EGR (Fig. 7). The latter difference could indicate a limitation of the model in describing the flame burn-out phase. However, it must be taken in mind that the MFB10-90 angle is generally affected by some uncertainties in the heat release calculation and normalization. Overall, the model is able to capture the EGR effect on the combustion angles, as the results in the second and third case were obtained with the same ECFM model constants. This is a quite significant results and supports the reliability of the LFS submodel in capturing the combustion-velocity trend versus EGR content. The latter conclusion is even more apparent if the heat release time-histories of the case without EGR (Fig. 8) is compared to that obtained for the case with EGR=20% (Fig. 9). It is also worth mentioning that the calculated pressure at SA is about 4% higher than the experimental pressure, both in the case without EGR and in the case with EGR. This might indicate a slight inaccuracy in the heat transfer modeling during the compression phase. However, such an error has been considered acceptable.

Results and discussion

Preliminary results.

As mentioned above, as a first step of the engine development phase, the combustion chamber was re-designed in order to increase the mechanical resistance. A peak pressure of 180 bar could finally be allowed for the ‘upper’ cycles (average maximum pressure ‘+ 2σ’), as well as to improve the in-cylinder turbulence characteristics. Consequently, the chamber and intake port geometry had to be verified by calculation before the single cylinder engine realization and assembly.

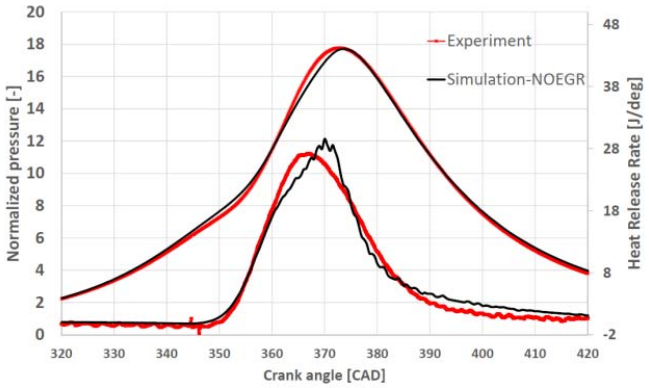

Figure 8. CFD model validation: pressure cycle and heat release @2000 rpm , imep = 8 bar, without EGR.

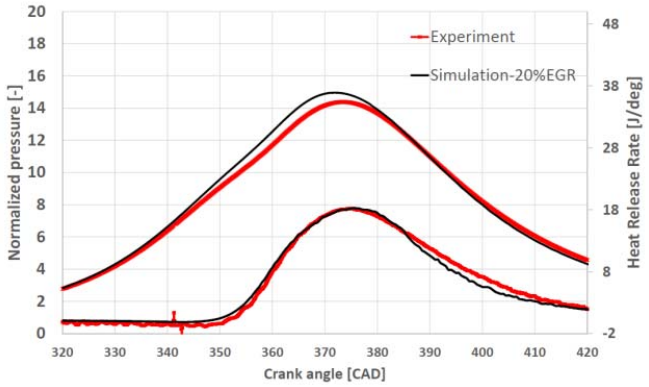

Figure 9. CFD model validation: pressure cycle and heat release @2000 rpm , imep = 8 bar, EGR = 20%.

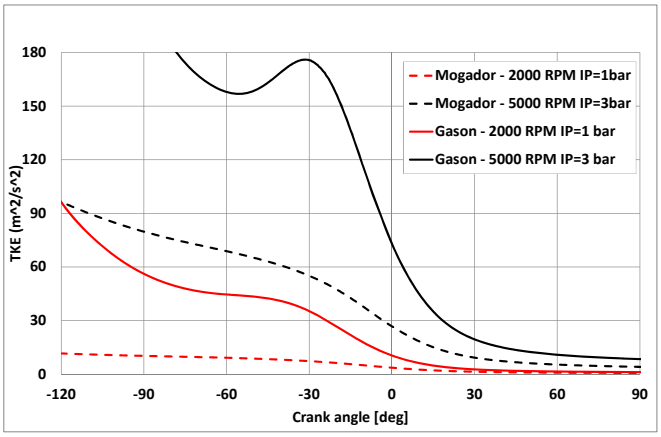

Figure 10. Turbulent kinetic energy (TKE) from the Gason engine vs. Mogador, in two different working conditions.

Figure 10 shows the results of the preliminary analysis, which was carried out by Renault by means of a cold-flow CFD model developed in CONVERGE. The chart reports the time-history of the turbulent kinetic energy for two considered working conditions, namely, 2000 rpm and average intake pressure (IP) fixed at 1 bar (red color), and 5000 rpm and IP fixed at 3 bar (black curves). It is worth considering that, in the absence of the combustion process, it is not possible to precisely define the engine load. Based on the induced air flow rate amount, IP = 1 bar corresponds to a medium load condition, whereas IP = 3 bar can be considered as a full-load operating point. Besides, the turbulence patterns from the Gason engine (solid lines) have been compared to those obtained for the Mogador one. The turbulence level is much higher for the Gason engine, as the TKE at 0 deg (closed-valve TDC) is 2.7 to 3 times than the Mogador engine. This is due to a higher tumble intensity and turbulence production during the intake and compression strokes. Moreover, the more apparent tumble structure is subject to a higher spin-up effect during the late compression stroke and to the subsequent decay towards TDC [26, 30]. The remarkable increase in turbulence intensity can promote the combustion process, by increasing the engine thermal efficiency and by decreasing the cycle-to-cycle variation, thus allowing an increase in the EGR tolerance of the engine [6, 33].

Experimental results.

In order to characterize the effect of EGR on engine combustion and performance, tests were carried out at IFPEN by adopting the layout shown in Fig. 2. The tests were conducted at the engine speed of 2000 rpm, at different engine loads, without EGR and with EGR=20% on a mass basis. The most significant engine variables of the presented tests are reported in Table 6.

Table 6. Summary of the experimental cases presented in the paper.

Case [rpm x bar]	Spark advance [CA BTDC]		Injection time [CA BTDC]		Boost level [bar]	
	EGR = 0%	EGR = 20%	EGR = 0%	EGR = 20%	EGR = 0%	EGR = 20%
2000 x 3	19	23	260	260	0.43	0.55
2000 x 4.6	17	24.5	260	260	0.57	0.68
2000 x 8	16	19	260	260	0.85	1.06
2000 x 9.6	16	21	260	260	0.98	1.21
2000 x 31.5	9	12	260	260	2.85	3.15

The main results of the experimental campaign are reported in Fig. 11. In the performed test the addition of 20% external EGR led to an apparent reduction of the pumping work, as is testified by the low-pressure imep values (LP-imep, Fig. 11a). The latter are due to a substantial engine de-throttling. In fact, by approximately considering constant air and fuel rates for a given load, a higher intake pressure is required when the fresh charge is diluted with external EGR. Figure 11b reports the comparison of the combustion phasing, as it is defined by the MFB50 position. This latter was evaluated a posteriori by performing a single-zone heat release analysis on a cycle to cycle basis and by averaging the cycle-resolved MFB50 values. As can be inferred from the plot, a non-optimal combustion phasing was obtained in the EGR case. This was due to the increased cyclic variability of the engine, and the consequent difficulty in properly detecting the combustion phasing in real time. Moreover, given the single cylinder nature of the engine, the more apparent vibrations did not allow the fine tuning of the spark advance case by case. At full load the SA was mainly limited by the maximum peak firing pressure, which imposed an apparent retard of the combustion phasing for both EGR and no-EGR working conditions. As far as the

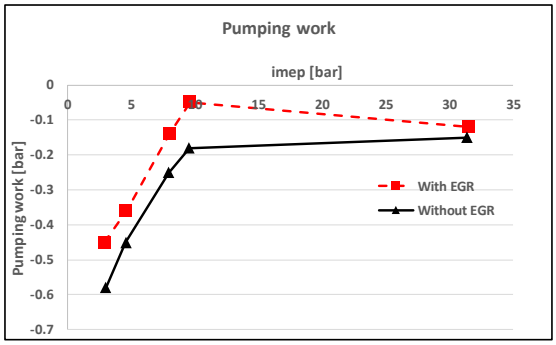

(a)

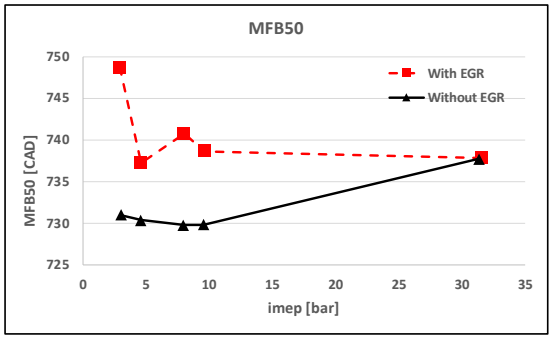

(b)

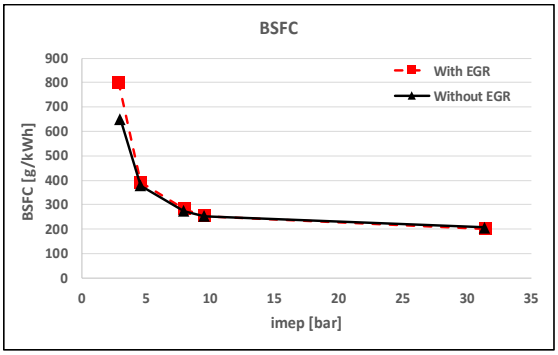

(c)

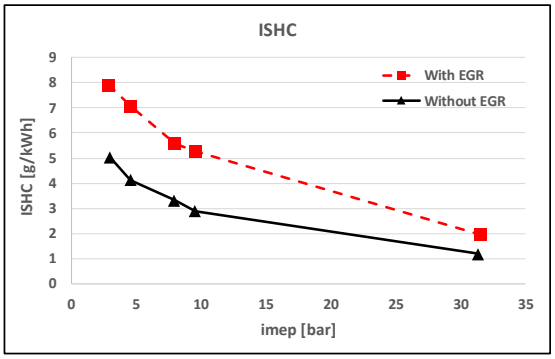

(d)

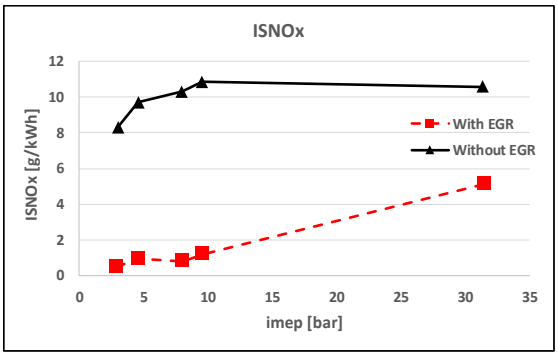

(e)

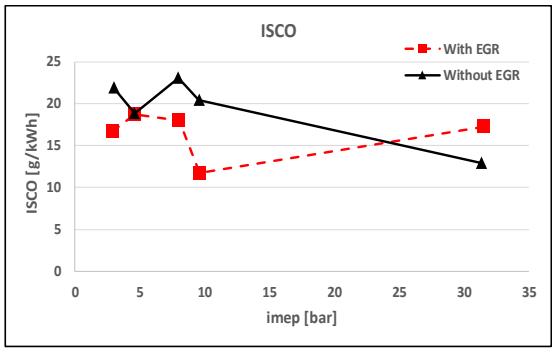

(f)

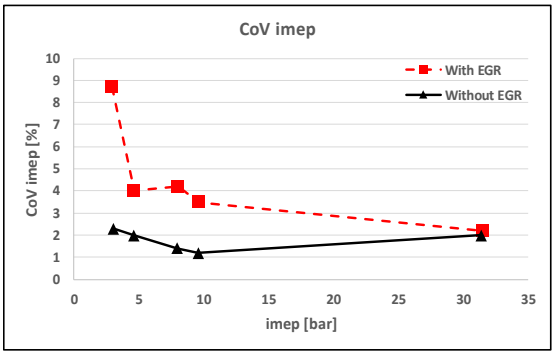

g)

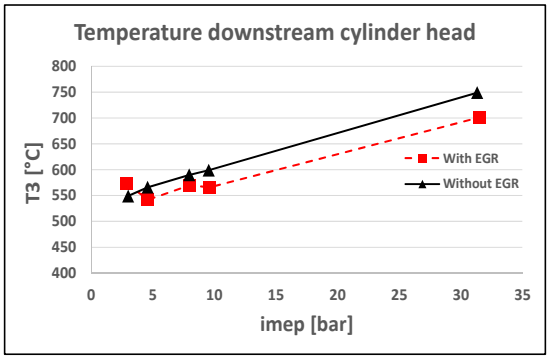

(h)

Figure 11. Experimental results at 2000 rpm for different engine loads.

fuel consumption is concerned (BSFC, Fig. 11c), the results obtained are mainly a combined effect of the LP-imep and MFB50 behavior. More specifically, with the only exception of the full-load conditions, the negative effect caused by the non-optimal combustion timing overcomes the benefits induced by the reduction in the pumping losses. On the other hand, the combustion phase is virtually the same at full load, leading to a benefit in the fuel consumption of about 3%. This is consistent with the findings in [7].

The effect of EGR on the engine specific emissions is shown in Figs. 11d, 11e and 11f. On an average, the obtained results are consistent with the expected ones, as an HC increase of about 70% and a NOx decrease from 50 to 90% was obtained with diluted combustion. Figure 11g shows the effect of EGR on the engine stability, as represented by the coefficient of variation of the engine imep. At very low load, the decrease in burning velocity due to the charge dilution is more apparent and the CoV increases up to 9%, which is definitely not feasible for a vehicle application. The effect of EGR on the cycle-to-cycle combustion variation decreases as load increases. This is promising in view of a possible implementation of a diluted-combustion strategy at full load, although further investigation is needed to verify the results in the multi-cylinder engine layout and to optimize the engine calibration. As a matter of fact, the EGR tolerance is most likely affected by the SA adopted, as well as by the charge homogeneity. The latter in turn depends on the direct injection phasing and duration. The chart in Fig. 11h shows that the adoption of EGR leads to a decrease in the turbine-inlet temperature of about 20-50 K, with the only exception of the case at imep=3 bar. It should be also considered that the benefit can be increased by a suitable advance of the combustion with respect to the current setting (Fig. 11b).

CFD results (EGR sweeps).

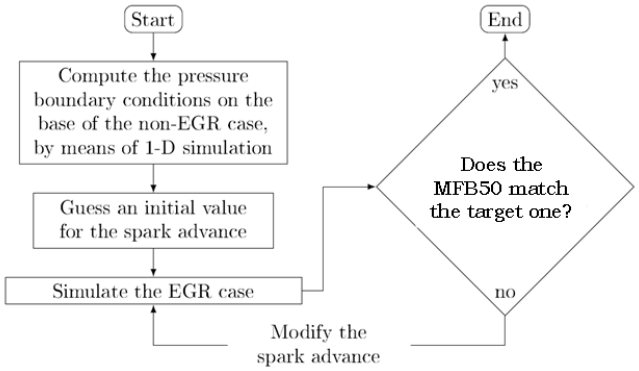

Figure 12. Procedure adopted for the EGR-sweep CFD simulation.

In order to gain additional insight into the engine combustion and performance dependence on the EGR rate, a series of EGR sweeps were setup and carried out, by using the CFD model described above. More specifically, with reference to a few selected engine working points, the performance and fluid-dynamic variables obtained without EGR were taken as reference, and the EGR percentage has been varied by keeping the combustion phasing and the imep value unchanged. An 'optimal' combustion timing condition set as target, in which the MFB50 was fixed to 728 ±2 deg CA. Moreover, in order to get rid of the possible dependence of the combustion behavior on the mixture homogeneity, a uniform mixture hypothesis was considered in the simulations both in the absence and in the presence of EGR. Also, in order to reproduce the case of ideally cooled EGR, the intake temperature was kept constant for the various EGR rates considered.

Figure 12 summarizes the procedure which was applied to the EGR sweep simulation. First, a GT-Power model of the single-cylinder engine was used to derive the boundary conditions to be used for the 3-D CFD model. For each of the considered working points, several simulations were performed with increasing EGR content and, for each of them, the engine inlet pressure was calibrated by targeting the engine imep, by using the GT-Power Optimizer feature. Second, the obtained boundary conditions were used as input for the simulations in the presence of EGR, and a tentative value of the spark-timing was set for running the model. Since the effect of the EGR rate on the burning speed was not known a priori, the choice of the spark advance needed to be verified against the target. Moreover, given the quite apparent sensitivity of the simulated results of the first cycle to the initial conditions, and taking the cycle-to-cycle variation of the simulated results, the model was run for at least three cycles and the average between the MFB50 from cycle no. 2 and 3 was checked against the target. In the case of agreement within the tolerance of ±2 deg CA, the simulation was run until cycle no. 7 in order to decrease the effect of the numerical cyclic dispersion on the results. Otherwise, the case was stopped and run again with a modified spark advance.

The simulated cases and their respective SA values are reported in Table 7. The percentage of EGR is also indicated in the table: the notation 'EGR' actually refer to the external EGR, whereas 'Overall EGR' indicates the sum of the external EGR and the residual gases which remain in the cylinder at EVC. It is worth noting that, since the engine intake pressure increases as EGR rate increases, the residual gas percentage (i.e. the difference between overall and external EGR) decreases. As will be clear in what follows, as the combustion behavior is actually affected by the overall EGR, the residual-gas amount directly affects the maximum allowed external EGR rate for each working condition.

Table 7. EGR sweep: summary of simulated cases .

Case [rpm x bar]	EGR [%]	Overall EGR (ext.+res.) [%]	SA [deg]	boost [bar]
2000 x 3	0	17	19	0.43
	20	30	29	0.49
	25	32	44	0.51
	30	36	44	0.53
2000 x 8	0	8.7	16	0.85
	20	25	31	0.98
	30	32	41	1.07
	35	36	46	1.12
3000 x 8	0	6.7	22	0.82
	30	32	50	1.16

The results of the numerical study are reported hereafter. Figures 13-16 show in detail the engine behavior for the case at 2000 rpm, imep = 8 bar, whereas Figs. 17,18 give a general overview of the EGR impact on the most significant combustion and performance-related variables.

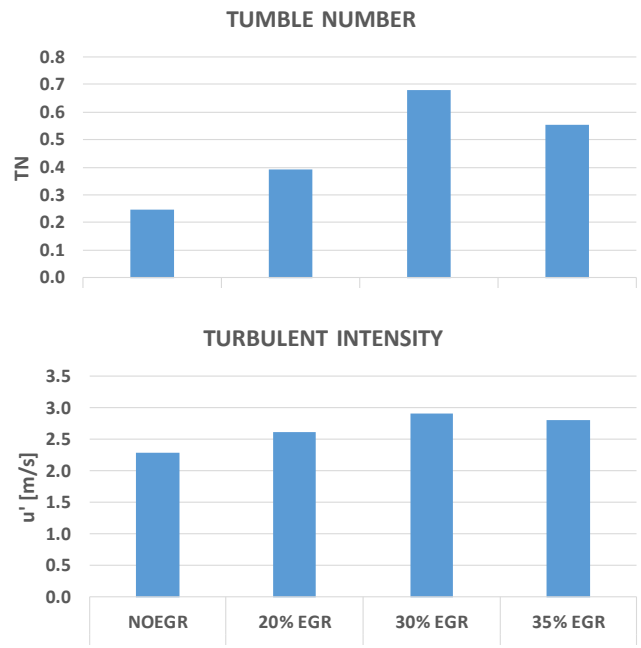

Figure 13. Tumble number and turbulence intensity at spark timing @2000 rpm, imep=8 bar, for different EGR rates.

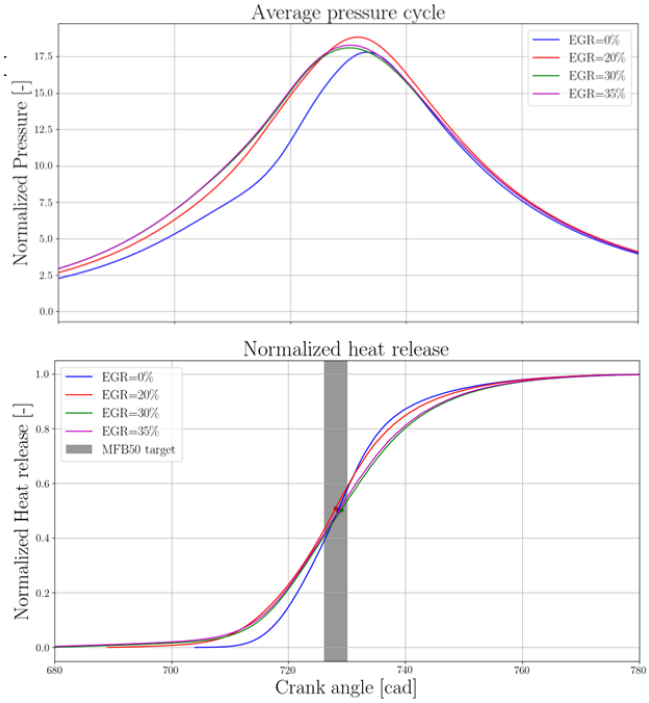

Figure 14. Average pressure cycle and heat release profile for different EGR rates at 2000 rpm, imep = 8 bar.

As far as the charge motion and turbulence is concerned, a detailed analysis would show that the charge inlet velocities share nearly the same values during the induction phase. Such an analysis has been omitted for the sake of brevity. Consistently, the time-history of the tumble number and turbulence intensity is almost equivalent for different EGR rates. Since the spark advance is increased as the EGR increases (see Table 7), the tumble number and the turbulence intensity at SA consistently increase, with the only exception of EGR= 35% (Fig. 13). Overall, the turbulence intensity at the beginning of the combustion ranges between 2.2 and 2.8 m/s, which is a fully satisfactory value from the point of view of the combustion enhancement, also considering the rather low engine speed under study. Figure 14 compares the in-cylinder pressure evolution and the normalized heat release profiles obtained from the simulations. As the EGR content is increased, the pressure during the compression phase increases, due to the rise in the intake pressure which is required to keep the engine load constant. The heat release plot (lower chart in Fig. 14) shows that the burning rate is negatively affected by the charge dilution, consistently with the apparent detriment in laminar burning speed caused by the EGR (see Fig. 5). The maximum slope of the curve decreases by around 30% by changing the external EGR from 0 to 30%. The behavior of the heat release determines a slower pressure rise during the combustion phase, so that a roughly constant peak firing pressure is finally obtained (upper chart in Fig. 14). Figure 15 shows the contour plots of fuel concentration in the valve section plane, for different EGR concentrations and at the same crank angle relative to the spark timing, namely, 30 deg CA after ST. The star indicates the spark position in each picture, which is located in a plane behind the section plane. The contour colorscale limits were fixed in such a way that the blue color corresponds to the burned-gas region and the red indicates the unburned one. In the last picture, due to the lower overall methane content, the unburned region falls into the orange color. In the absence of external EGR, the combustion process has been completed by 30 deg after SA, as only a very small quenching region presents a residual methane content. The burned gas region has a lower and lower size as the EGR is increased, and this indicates that the burned-gas radius has been reduced. The figure also shows that the combustion product region is displaced towards the exhaust side by the positive (clockwise) tumble component. Figure 16 reports the maximum burned and unburned-gas temperatures for the different cases at 2000 rpm and imep = 8 bar. Although the precise numbers actually depend on the interaction between flame speed, spark advance and mixture dilution, an overall decreasing trend is apparent. In particular, the maximum burned temperature decreases by around 20%. This is consistent with the much lower NOx emissions that have been experimentally detected, and is quite promising in the perspective of containing the exhaust temperatures, with specific reference to full-load conditions. It should be kept in mind that, for a given amount of fuel induced by the engine, lower exhaust temperatures generally lead to a higher engine thermodynamic efficiency.

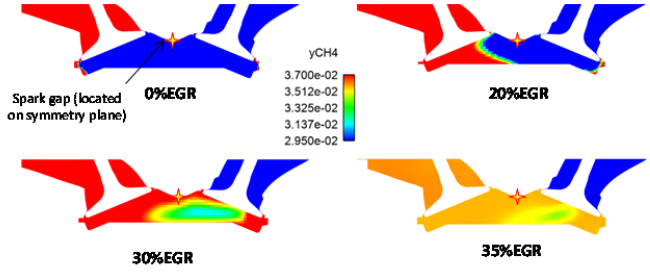

Figure 15. Isocurves of methane concentration at θ = 30 deg CA after ST (n = 2000 rpm, imep=8 bar). The star indicates the spark gap location (onto a plane behind the valve section plane).

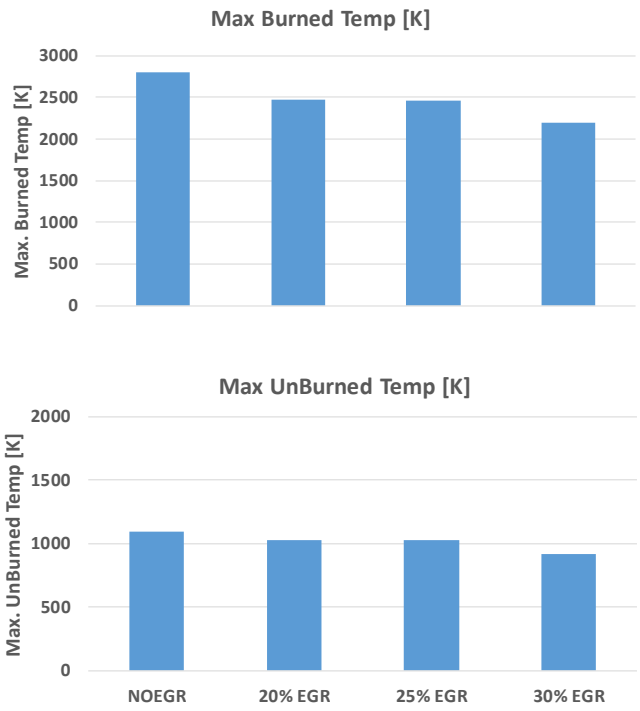

Figure 16. Burned- and unburned-gas temperatures @2000 rpm, imep=8 bar, from CFD simulations, for different EGR rates.

Figures 17 and 18 provide a general overview of the combustion behavior for different EGR rates. More specifically, Fig. 17 shows the obtained PFP and imep values in the various simulated test cases and EGR contents, and the main combustion-related quantities are shown in Fig. 18. These figures provide a quantitative evaluation of the influence of the mixture dilution on the combustion process and on the engine performance, along with several other tests performed at constant boost level and different spark timings, not included in the paper. From this evaluation, the engine EGR tolerance in the different conditions can be estimated. The tests performed show that, as the EGR rate is increased by trying to keep the imep and the MFB50 constant, the following results are obtained:

- The peak firing pressure turns out to be approximately constant, as a combined effect of the higher spark advance, the increased boost level and of the decreased combustion velocity;
- The combustion duration increases, though the effect is more apparent for the MFB0-50 interval than the MFB10-90 one. Similar results were obtained experimentally in [7, 9]. On an average, as the external EGR rate increases from 0 to 30%, the increase in MFB0-50 and MFB10-90 are between 90% and 100%, and between 35% and 40%, respectively.
- Within the EGR range corresponding to a sufficiently stable combustion process, it is found that the imep penalty, which is caused by the charge dilution, can be effectively recovered by the increase in the boost level.
- For a given boost level, the increase in the spark advance can lead to a more advanced MFB50 absolute position, and can also help in recovering the imep level. However, as EGR is gradually increased, the combustion process quickly switches from a stable evolution to a largely incomplete process, and finally to a misfire. It is was found that this switch often happens when the MFB0-50 interval is beyond 50 deg, and in such conditions the SA is between 45 and 50 deg. A further increase in the SA is virtually ineffective.

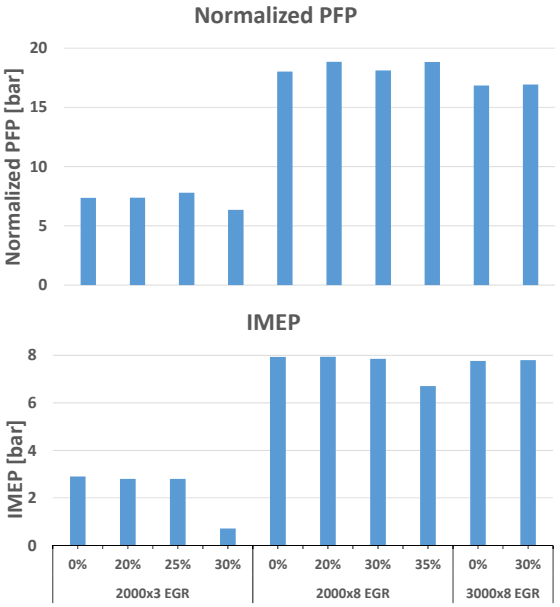

Figure 17. Peak firing pressure and imep values at different working points and for different EGR rates.

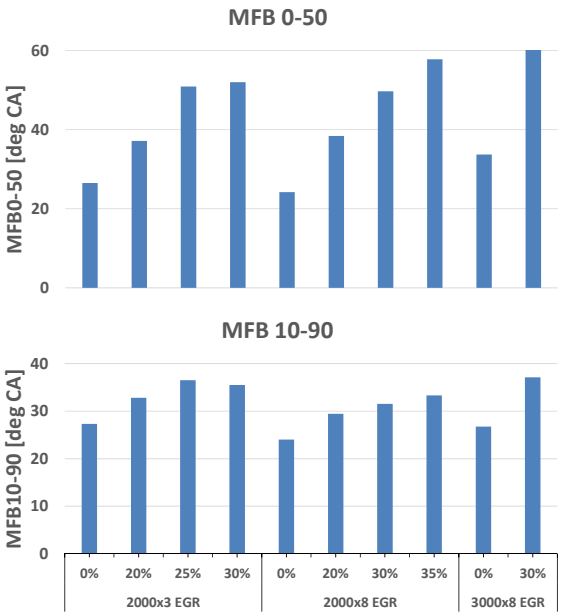

Figure 18. MFB50 and MFB10-90 values at different working points and for different EGR rates.

Concerning the attainment of the maximum allowed external EGR percentage, the precise evaluation is rather difficult and sometimes questionable, however, some general guidelines can be drawn on the basis of the results provided by the present numerical model. With specific reference to Figs. 17 and 18:

- Case 2000x3: the limit value MFB0-50 = 50 deg is reached for external EGR = 25%, which corresponds to overall EGR = 32%. Under these conditions, the combustion is still stable and the

imep decrease with respect to the target is acceptable. A higher overall EGR content immediately triggers an apparent combustion incompleteness (see Fig. 17, fourth case from left).

- Case 2000x8: the already mentioned limit value is reached, based on Table 7 and Fig. 18, for the same value of overall EGR, that is, 32%. With respect to the previous case, however, the change towards misfire conditions is slower, most likely due to the higher in-cylinder pressure and, consequently, the higher reactant concentration in the spark plug gap. Consequently, the EGR level of 35% (overall EGR = 36%) can be considered acceptable.
- Case 3000x8: a stable combustion is obtained up to an EGR rate of 30% (overall EGR = 32%), however, due to the lower time frame the increase in MFB0-50 is higher than in the 2000 rpm case. It follows that EGR = 30% can be considered as the limit conditions for the 3000x8 case.

Summary/Conclusions

In this paper a deep insight was given into the effect of the charge dilution by LP-EGR on performance and combustion parameters of a direct injection SI engine, specifically designed for CNG fueling. The activity was carried out within the Gason research project and included both an experimental work and CFD simulations.

The experimental activity has evidenced the potential of EGR to increase the engine efficiency, by allowing to increase the boost level at full load and by reducing pumping losses at partial load. A decrease in the engine exhaust temperature between 20 and 50 K was obtained, which is promising from the perspective of increasing the boost level at intermediate speeds. further reduction can be obtained by further optimizing the spark timing for EGR operation.

The CFD activity led to the development of a model which showed to be able to accurately describe the combustion process and its dependence on the in-cylinder turbulence. Moreover, the implementation of a LFS model based on detailed kinetics allows the trend versus EGR of the main combustion parameters to be captured. Given that the model results are in agreement with the experimental findings in the literature, it can be considered as a reliable predictive tool for the analysis of NG SI engine combustion under different dilution levels.

In the present investigation, the combustion model coefficients were kept fixed, in order to analyze the combustion process at different EGR rates and to identify the maximum allowed EGR rate of the engine under study. The maximum EGR rate can be identified in correspondence to a threshold value of the MFB0-50 interval, which can be fixed around 50-60 deg CA. For example, at 2000x8 the maximum EGR rate is around 35%. In general, the maximum rate showed an increasing trend versus load, due to the increasing reactant concentration in the spark plug gap. It also demonstrated a decreasing trend against the engine speed, due to the lower time available for the combustion process.

References

1. Cho, H.M. and He, B.Q., “Spark Ignition Natural Gas Engines – a Review,” Energy Conv. and Management 48:608-618, 2007, doi:10.1016/j.enconman.2006.05.023.
2. Korakianitis, T., Namasivayam, A.M., and Crookes, R.J., “Natural-Gas Fueled Spark-Ignition (SI) and Compression-Ignition (CI) Engine Performance and Emissions,” Progress in Energy and Combustion Science 37(1):89-112, 2011, doi:10.1016/j.pecs.2010.04.002.
3. Sobiesiak, A. and Zhang, S., “The First and Second Law Analysis of Spark Ignition Engine Fuelled with Compressed Natural Gas,” SAE Technical Paper 2003-01-3091, 2003, doi:10.4271/2003-01-3091.
4. Borges, L., Hollnagel, C., and Muraro, W., “Development of a Mercedes-Benz Natural Gas Engine M 366 LAG, with a Lean Burn Combustion System,” SAE Technical Paper 962378, 1996, doi:10.4271/962378.
5. GASON project website: http://www.gason.eu/
6. Zhang Z, Zhang H, Wang T, et al. Effects of tumble combined with EGR (exhaust gas recirculation) on the combustion and emissions in a spark ignition engine at part loads. Energy 2014;65(1):18–24.
7. Zoldak, P. and J. Naber, “Spark Ignited Direct Injection Natural Gas Combustion in a Heavy Duty Single Cylinder Test Engine - AFR and EGR Dilution Effects”. SAE Technical Paper 2015-01-2808, 2015, doi:10.4271/2015-01-2808.
8. G.P. McTaggart-Cowan., S.N. Rogak., S.R. Munshi., P.G. Hill., W.K. Bushe., “The influence of fuel composition on a heavy-duty, natural gas direct-injection engine”. Fuel 89 (2010) 752 – 759. doi: 10.1016/j.fuel.2009.10.007.
9. Morteza Fathi., R. Khoshbakhti Saray., M.David Checkel. “The influence of Exhaust Gas Recirculation (EGR) on combustion and emissions of n-heptane/Natural gas fueled Homogeneous charge compression ignition (HCCI) engine”. Applied Energy 88 (2011) 4719-4724.
10. Tanoue, K., Kuboyama, T., Moriyoshi, Y., Hotta, E. et al., "Extension of Lean and Diluted Combustion Stability Limits by Using Repetitive Pulse Discharges," SAE Technical Paper 2010-01-0173, 2010, https://doi.org/10.4271/2010-01-0173.
11. Hayashi, N., Sugiura, A., Abe, Y., and Suzuki, K., "Development of Ignition Technology for Dilute Combustion Engines," SAE Int. J. Engines 10(3):984-995, 2017, https://doi.org/10.4271/2017-01-0676.
12. Douailler B et al. Direct injection of CNG on high compression ratio spark ignition engine: numerical and experimental investigation. SAE technical paper 2011-01-0923; 2011.
13. Baratta M et al. Numerical and experimental analysis of mixture formation and performance in a direct injection CNG engine. SAE technical paper 2012-01-0401, 2012.
14. Baratta, M., Misul, D., Xu, J., Fuerhapter, A. et al., "Development of a High Performance Natural Gas Engine with Direct Gas Injection and Variable Valve Actuation," SAE Int. J. Engines 10(5):2017, https://doi.org/10.4271/2017-24-0152.
15. Peters N., Turbulent combustion, Cambridge University Press, 2009.
16. Colin O, Benkenida A., “Le modèle ECFM3Z (3-Zones Extended Coherent Flame Model) pour le calcul de la combustion par flammes de prémélange et flammes de diffusion The 3-Zones Extended Coherent Flame Model (Ecfm3z) for Computing Premixed/Diffusion Combustion”, Oil & Gas Science and Technology - Rev. IFP 59 (6) 593-609 (2004).
17. Bartolucci, L., et al., Natural Gas Partially Stratified Charge Combustion: Extended Analysis of Experimental Validation and Study of Turbulence Impact on Flame Propagation. SAE International, 2016. 1.
18. Bartolucci, L., et al., Partially Stratified Charge Natural Gas Combustion: The Impact of Uncertainties on LES Modeling. 2015. 1.
19. Bartolucci, L., et al., CFD and X-Ray Analysis of Gaseous Direct Injection from an Outward Opening Injector. SAE International, 2016. 1.

20. Colin O., Truffin K., “A spark ignition model for large eddy simulation based on an FSD transport equation (ISSIM-LES)”, n Proc. of the Combustion Institute, Volume 33(2), pp. 3097-3104, 2011.
21. http://combustion.berkeley.edu/gri-mech/version30/text30.html.
22. Gülder, Ö., "Correlations of Laminar Combustion Data for Alternative S.I. Engine Fuels," SAE Technical Paper 841000, 1984.
23. Metghalchi M., “Burning Velocities of Mixtures of Air with Methanol, Isooctane, and Indolene at High Pressure and Temperature”, Comb. and Flame 48, pp. 191-210, 1982.
24. Hu E., Huang Z., He J. et al. “Experimental and numerical study on laminar burning characteristics of premixed methane–hydrogen–air flames”, Int. J. of Hydrogen energy 34, pp.4876-4888, 2009.
25. http://ignis.usc.edu/USC_Mech_II.htm.
26. Hu,E., Li, Xiatian., Meng, Xin., Chen, Yizhen., Cheng, Yu., Xie, Yongliang., Huang, Z., “Laminar flame speeds and ignition delay times of methane-air mixtures at elevated temperatures and pressures”. Fuel 158 (2015) 1-10.
27. J. Huang., P.G. Hill., W.K. Bushe., S.R. Munshi., “ Shock tube study of methane ignition under engine relevant conditions: experiments and modelling”. Combustion and flame 136 (2004) 25-42.
28. Nicola Donohoe., Alexander Heufer., Wayne K.Matcalfe., Henry J. Curran., Marissa L. Davis., Olivier Mathieu., Drew Plichta., Anibal Morones., Eeric L. Petersen., Felix Güthe. “ Ignition delay times, Laminar flame speeds and mechanism validation for natural gas/hydrogen blends at elevated pressures”. http://dx.doi.org/10.1016/j.combustflame.2013.12.005.
29. Rathinam, B., Ravet, F., Servant, C., Delahaye, L. et al., "Experimental and Numerical Investigations of Tumble Motion on an Optical Single Cylinder Engine," SAE Technical Paper 2015-01-1698, 2015.
30. Scarcelli, R., Matthias, N.S., Wallner, T., “Numerical and Experimental Analysis of Ignition and Combustion Stability in EGR Dilute GDI Operation”, ASME Paper ICEF2014-5607, ASME 2014 ICED Fall Technical Conference, 2014.
31. Scarcelli, R., Richards, K., Pomraning, E., Senecal, P.K., Wallner, T., Sevik, J., “Cycle-to-Cycle Variations in Multi-Cycle Engine RANS Simulations”, SAE Technical Paper 2016-01-0593, 2016.
32. Brunt, M.F.J., Rai, H., Emtage, A.L., “The Calculation of Heat Release Energy from Engine Cylinder Pressure Data,” SAE paper No. 981052, 1998.
33. Baratta, M., Misul, D., Spessa, E., et al. “Experimental and numerical approaches for the quantification of tumble intensity in high-performance SI engines”, Energy Conversion and Management 138, pp. 435–451, 2017.

Contact Information

MIRKO BARATTA
Dipartimento Energia, Politecnico di Torino
Corso Duca degli Abruzzi 24
10129 Torino – Italy
mirko.baratta@polito.it
+39 011 090 4484

Acknowledgments

This work has been performed with the financial support of the Gason project of the EC, H2020 program. The support of Convergent Science GmbH, Linz, Austria in providing the CONVERGE software and in supporting the model development is acknowledged.

Definitions/Abbreviations

λ	Relative A/F ratio
CA	Crank angle
CNG	Compressed natural gas
Deg	degree
EGR	Exhaust gas recirculation
imep	Indicated mean effective pressure
IP	Intake pressure
LFS	Laminar flame speed
LP	Low-pressure
MCE	Multi-cylinder engine
MFB	Mass-fraction burned
NG	Natural gas
SA	Spark advance
SCE	Single-cylinder engine
ST	Spark timing
TDC	Topdead center
TKE	Turbulent kinetic energy
VVT	Variable valve timing